Longitudinal changes in cortical thickness associated with normal aging

Madhav Thambisetty [a],[*], Jing Wan [b], Aaron Carass [b], Yang An [a], Jerry L. Prince [b], Susan M. Resnick [a]

[a] Laboratory of Personality and Cognition, National Institute on Aging, Baltimore, MD, USA
[b] Department of Electrical and Computer Engineering, The Johns Hopkins University, Baltimore, MD, USA

ARTICLE INFO

ABSTRACT

Imaging studies of anatomic changes in regional gray matter volumes and cortical thickness have documented age effects in many brain regions, but the majority of such studies have been cross-sectional investigations of individuals studied at a single point in time. In this study, using serial imaging assessments of participants in the Baltimore Longitudinal Study of Aging (BLSA), we investigate longitudinal changes in cortical thickness during aging in a cohort of 66 older adults (mean age 68.78; sd. 6.6; range 60–84 at baseline) without dementia. We used the Cortical Reconstruction Using Implicit Surface Evolution CRUISE suite of algorithms to automatically generate a reconstruction of the cortical surface and identified twenty gyral based regions of interest per hemisphere. Using mixed effects regression, we investigated longitudinal changes in these regions over a mean follow-up interval of 8 years. The main finding in this study is that age-related decline in cortical thickness is widespread, but shows an anterior–posterior gradient with frontal and parietal regions, in general, exhibiting greater rates of decline than temporal and occipital. There were fewer regions in the right hemisphere showing statistically significant age-associated longitudinal decreases in mean cortical thickness. Males showed greater rates of decline in the middle frontal, inferior parietal, parahippocampal, postcentral, and superior temporal gyri in the left hemisphere, right precuneus and bilaterally in the superior parietal and cingulate regions. Significant nonlinear changes over time were observed in the postcentral, precentral, and orbitofrontal gyri on the left and inferior parietal, cingulate, and orbitofrontal gyri on the right.

Published by Elsevier Inc.

Introduction

Neuroimaging methods to assess brain atrophy have been extensively applied to track the onset and progression of neurodegenerative conditions such as Alzheimer's disease (AD) (Callen et al., 2001; De Santi et al., 2001; Du et al., 2001; Soininen et al., 1994). Longitudinal analyses have proven especially useful in delineating changes in brain volume during normal aging (Resnick et al., 2003), as well as in evaluating the temporal progression of neuropathology in AD (Driscoll et al., 2009; Fox et al., 2000; Jack et al., 2004; Misra et al., 2009; Mungas et al., 2005; Schott et al., 2005). In older individuals, longitudinal decreases in gray and white matter volumes are widespread, and these declines are observed even in very healthy subjects during normal aging (Resnick et al., 2003). In AD, the rates of whole brain atrophy are several times greater than age-matched controls and differentiate the two groups with sensitivity greater than 90% (Fox and Freeborough, 1997). Medial temporal lobe structures such as the hippocampus and entorhinal cortex are especially vulnerable to

early atrophic changes in AD (Du et al., 2004; Du et al., 2003; Jack et al., 2004), and accelerated longitudinal tissue loss in these structures has been shown to precede the onset of cognitive impairment in subjects at risk (Fox et al., 1996).

We have recently shown that spatial patterns of regional atrophy provide better discrimination between MRI scans of cognitively normal and impaired individuals than a global or single regional atrophy measure alone (Davatzikos et al., 2008a). Moreover, these high-dimensional pattern classification approaches may have additional utility in the differentiation between sub-types of dementia (Davatzikos et al., 2008b). Subsequently, others have reported concordance between patterns of spatial atrophy detected in ante-mortem MRI studies and the distribution of neurofibrillary pathology in the brain at autopsy (Whitwell et al., 2008).

Recent studies suggest that the measurement of cortical thickness in vulnerable brain regions may also be a useful tool to detect perturbations in brain structure in cognitively normal subjects at risk for development of AD (Burggren et al., 2008) and in subjects with mild cognitive impairment (MCI) (Singh et al., 2006). Furthermore, decreases in cortical thickness appear to correlate well with severity of clinical impairment even in the earliest stages of AD (Dickerson et al., 2008). These data indicate that cortical thickness may represent a more sensitive, and perhaps complementary, measure of early pathological change than standard MRI-based volumetry in

* Corresponding author. BRC – Biomedical Research Center, 04B311, National Institute on Aging, 251 Bayview Blvd., Baltimore, MD 21224-2816, USA. Fax: +1 410 558 8674.
E-mail address: thambisettym@mail.nih.gov (M. Thambisetty).

subjects at risk for subsequent cognitive decline. However, these studies, while suggestive, are cross-sectional and are therefore limited in their ability to address the effects of age-related changes in cortical thickness over time.

We have previously reported cross-sectional age differences and 4-year longitudinal age changes in mean cortical thickness within eight sulcal regions in a subset of 35 older adults from the Baltimore Longitudinal Study of Aging (BLSA) (Rettmann et al., 2006). In a cross-sectional study that also included young and middle-aged individuals, global cortical thinning was detectable by middle age with similar patterns of age differences in cortical thickness in both males and females (Salat et al., 2004). In the present study, we extend these investigations of cortical thickness through analysis of longitudinal changes in 66 older BLSA participants with up to eight serial imaging assessments. Furthermore, we determine whether age and sex influence rates of change in cortical thickness in older individuals during normal aging.

Materials and methods

Subjects

This analysis included 66 individuals in the neuroimaging substudy of the BLSA (Resnick et al., 2000) all of whom completed at least 6 annual follow up scans. Most of these participants (60 individuals) completed 8 annual follow up scans. The sample included 38 males and 28 females, with 37 and 26 right-handed males and females, respectively, ranging in age at baseline from 60 to 84 years. The following exclusionary criteria were applied to all entrants at baseline; central nervous system disease (epilepsy, stroke, bipolar illness, prior diagnosis of dementia according to diagnostic and statistical manual-III-R criteria (American Psychiatric Association, 1987), severe cardiovascular disease (myocardial infarction, coronary artery disease requiring angioplasty, or bypass surgery), severe pulmonary disease, or metastatic cancer. All participants remained free of dementia throughout the duration of their involvement in the present study. The research protocol was approved by the local Institutional Review Board, and written informed consent was obtained from all participants in conjunction with each neuroimaging visit.

Image acquisition

The MRI acquisition of the brain volumes consisted of spoiled gradient echo (SPGR) volumetric magnetic resonance images, axially acquired, with the following parameters: TR = 35 ms, TE = 5 ms, flip angle = 45°, image matrix = 256 × 256, field of view = 24 cm, NEX = 1; and voxel dimensions 0.9375 × 0.9375 × 1.5 mm. Each data set was acquired on one of three GE Medical Systems Signa 1.5 T scanners (GE Healthcare, Waukesha, WI).

Cortical reconstruction

To reconstruct the cortical surface from acquired MR data, we used Cortical Reconstruction Using Implicit Surface Evolution (CRUISE) (Han et al., 2004; Xu et al., 2000). This method has undergone extensive validation which is detailed in Tosun et al. (2006). The CRUISE processing pipeline begins with a fuzzy tissue classification that is robust to noise and inhomogeneity artifacts (Pham, 2001). The classification provides three membership functions representing the fraction of WM, GM, and cerebrospinal fluid (CSF) present within a given voxel of the image. The next step creates masks of the ventricles and subcortical GM structures (e.g., putamen, thalamus) within the WM membership functions using Bazin and Pham (2007). Next, a triangulated surface mesh lying on the GM–WM boundary is computed as the 0.5 isolevel of the WM

membership function. Noise, partial volume effects, and scanner artifacts cause the WM isosurface to contain "holes" and "handles" which are removed using a graph based correction algorithm (Han et al., 2002). Because of the partial volume effect, opposing GM banks within narrow sulci are difficult to distinguish as separate banks. To address this problem, CRUISE automatically edits the GM membership function to create thin gaps between the banks of narrow sulci (Han et al., 2004; Xu et al., 2000). The final stage in CRUISE uses a topology preserving geometric deformable surface model (Han et al., 2003), initialized at the GM/WM surface, which is driven toward the pial surface using forces derived from the edited GM membership function. Figs. 1a–c show results of typical CRUISE processing of MRI data to generation of surfaces.

Reliability maps

Cortical surfaces are automatically labeled using the "reliability map" approach of Wan et al. (2008) which seeks to provide labels to regions that can be reliably labeled while leaving ambiguous regions unlabeled. The first step is to create a reliability map using a separate image database of labeled volumetric MRI scans (Desikan et al., 2006). The original data were T1-weighted magnetization prepared rapid gradient echo (MP-RAGE) volumetric scans comprising two sagittal acquisitions which were averaged to increase the contrast-to-noise ratio. The data were manually labeled within the image volumes yielding 33 labels per hemisphere; details can be found in Desikan et al. (2006). In early validation trials of our algorithm (see below) we found that several regions were inconsistently labeled, so we merged these regions with adjacent regions, forming a superset of 20 labels per hemisphere. Fig. 2 shows the surface labels on one of the atlas brains. Thirty four of these atlases were found to be complete and suitable for our use. We randomly split the collection of "Desikan" atlases into two groups, where the first group of 17 became the atlas database while the second group of 17 were used to validate the approach (Wan et al., 2008). The reliability map $R_A(v)$ for atlas brain A has values in the interval [0, 1] on each voxel v of A, describing how reliably this voxel can be deformably registered to a subject brain. We create $R_A(v)$ as follows:

Given $N(=17)$ atlases $A_1, A_2, \ldots, A_N$ with labels $L_i(v)$ on each voxel v we obtain $F_{A_i}(v)$ by deformably registering A_i against each of $A_1, \ldots, A_N$, (excluding A_i) using the Adaptive Bases Algorithm (ABA) (Rohde et al., 2003). We denote by A_{1i} the atlas A_1 deformably registered to atlas $A_i, i = 2, \ldots, N$. Then, $L_{1i}(v)$ is found by deforming $L_1(v)$ using the corresponding deformation field. The reliability $R_{A_1}(v)$ evaluates the degree of agreement of $L_{1i}(v)$ with $L_i(v)$, as follows

$$R_{A_1}(v) = \frac{\sum_{i=2}^{N} \delta(L_{1i}(v), L_i(v))}{N-1}, \tag{1}$$

where, $\delta(a, b)$ is the Kronecker delta. A reliability value of 1 at a given voxel means that that voxel has been mapped into the correct region (same label) for all $N - 1$ atlases. For each atlas we compute this reliability map relative to the other $N - 1$ atlases before labeling any subject not contained within the atlas. These reliability maps are defined on the atlas volumes, but can be mapped to any surface that happens to be defined within the volume. Fig. 3 shows a reliability map on a GM/CSF interface defined by CRUISE.

Labeling

For each atlas A_i we have labels $L_i(v)$ and the reliability map $R_{A_i}(v)$ for all voxels v of A_i. We label subject S using M atlases ($M \leq N$) as follows:

1. Register the M atlases to S and compute a voting score on each voxel that receives a given label. Let $L_{iS}(v)$ denote the result of
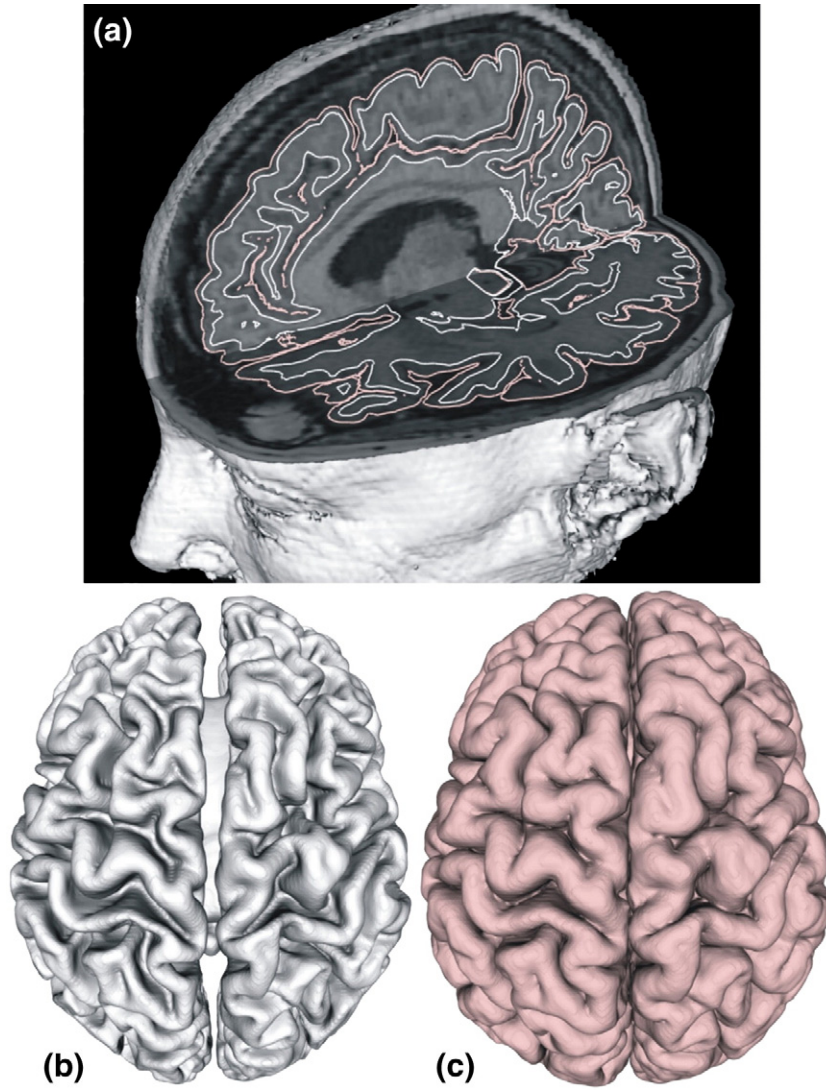
Fig. 1. (a) Cut-away of MR image of a whole head showing the inner (white outline) and outer (pink outline) cortical surface reconstructions. (b) Inner cortical surface. (c) Outer cortical surface. (d) Gyral regions over which thickness data is pooled.

transforming the labels $L_i(v)$ into S using the corresponding deformation field and $R_{iS}(v)$ denotes the transformed reliability map. $V_j(v)$ is the voting score that v receives the label j and is defined as follows

$$V_j(v) = \sum_{i=1}^{M} \delta(L_{iS}(v), j) R_{iS}(v), \qquad (2)$$

where $j=1,\ldots,K$, with K being the total number of labels in the atlas. For each voxel choose a candidate label l defined as $l = \text{argmax} \{j : V_j(v)\}$.

2. For the candidate label, compute the average reliability value,

$$R(v) = \frac{\sum_{i=1}^{M} \delta(L_{iS}(v), l) R_{iS}(v)}{\sum_{i=1}^{M} \delta(L_{iS}(v), l)}. \qquad (3)$$

We assign the label l to the voxel v if $R(v)$ is larger than a threshold t, otherwise we leave the voxel unlabeled. That is,

$$L_S(v) = \begin{cases} l, & \text{if } R(v) \geq t, \\ 0, & \text{otherwise.} \end{cases} \qquad (4)$$

We choose M in order to reduce the number of registrations required without affecting the accuracy of the results. In Wan et al. (2008) it was demonstrated that choosing $M=3$ yielded improvements over a traditional voting scheme with five atlases. It was also determined that use of the threshold $t=0.80$ yielded satisfactory results, so that is the value we use in the present work.

Thickness

We use the thickness estimation method described in Han et al. (2001) to compute cortical thickness. In this approach, cortical thickness is computed from the image volume using two distance transforms, one computed from the inner surface and one computed from the outer surface. A thickness value is assigned to each voxel in the volume between the two surfaces and is defined as the sum of the distances from the voxel to each of the two surfaces. The reconstructed central cortical surface is generated in the same coordinate space as the image volume, which means that each vertex of its surface mesh can obtain image values by directly mapping into the image data in the volume. Accordingly, we obtain measures of cortical thickness at each surface vertex of the central cortical surface using
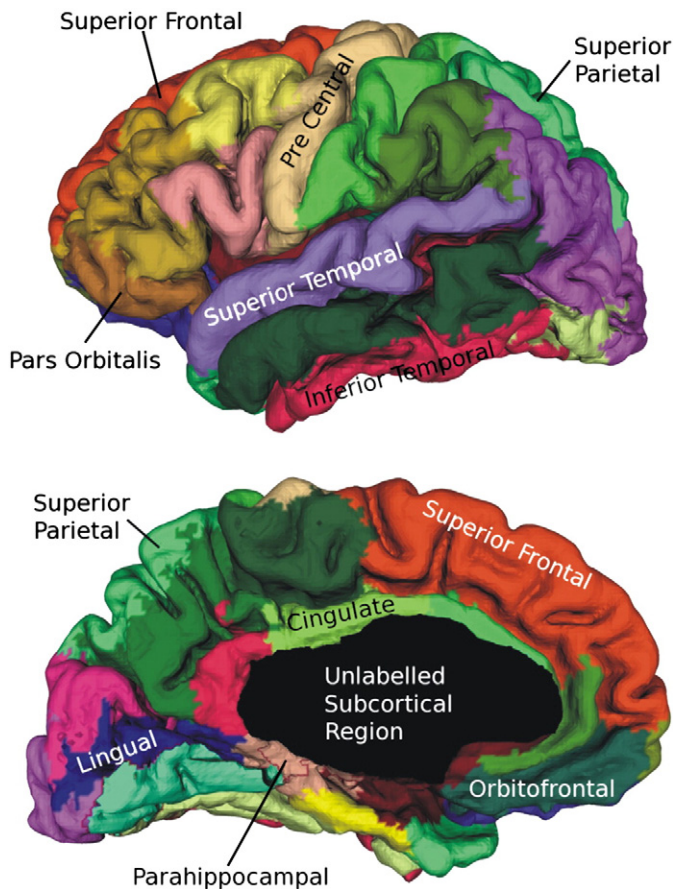
Fig. 2. Two views showing automatically generated gyral regions of interest. Some regions are labeled for reference.

trilinear interpolation applied in the image volume containing estimates of cortical thickness at volumetric grid points.

To test the repeatability of our thickness measures, we used the repeat scan data available from the Open Access Series of Imaging Studies (OASIS) project (Marcus et al., 2007). From the OASIS data pool we took ten subjects, each with two scans, and used the same processing steps to generate our thickness estimates for each of the regions of interest. We then did a test–retest analysis to determine the consistency of the measurements for a given subject. Test–retest correlation values range from −1.0 to 1.0, and values above 0.75 are considered to represent very good test–retest reliability. The values from our ten subjects were between 0.833 and 0.968, with an average test–retest correlation of 0.902. In addition, the mean intraclass correlation coefficient (ICC) (S.D.) across regions in these subjects was 0.6 (0.22). In our analysis of cortical thickness changes in aging, we analyze each volume independently in carrying out computations leading to cortical thickness measurements, and we use statistical analysis to analyze the resulting thickness data.

Statistical analysis

Linear mixed effects models were used in our analyses (Hartley and Rao, 1967; Laird and Ware, 1982). The main characteristic of the longitudinal data is that data points within each subject are correlated and mixed effects models take into account these correlations as part of the estimation process by including random effects, thus making the parameter estimates unbiased and more efficient. The models were fit using the lme function from the nlme package (Pinheiro and Bates, 2000) in R version 2.9.0.

We used the median thickness values for each of the 40 ROIs as our dependent variables. There were two goals in this longitudinal study;

i.e. characterization of the age-related growth–decline curve and estimation of longitudinal rates of change and sex differences in those changes. These goals were incorporated into the following analyses. We first used a backward elimination from a full model for each gyral region of age*sex and age*scanner which showed that the sex term was significant in some regions while the scanner term never reached significance. We therefore removed scanner as a potential predictor in all remaining analyses. In the next round of analyses, we fit linear mixed effects models with a quadratic functional form in age to the data. This allowed us to test if the observed longitudinal changes were linear or nonlinear. The fixed-effect part of this model included intercept, sex, age, age*age, and sex interactions with age and age*age as predictors. The initial random-effect part of the model included intercept, age, and age*age. In the subsequent round of analyses, we used models with linear longitudinal changes to estimate rates of change. The fixed-effect part of this model included intercept, sex, age, and sex*age as predictors. The initial random-effect part of the model included intercept and age. All the model reductions started from random effects. Non-significant random effects were dropped from the model.

The restricted maximum likelihood (REML) method was used in all models because it produces unbiased estimates of variance and covariance parameters. The age variable was centered at 60 and divided by 10. This means the intercept is the level at age 60 and change is measured in decades. Effect coding was used for the sex variable (−0.5 for females and 0.5 for males). This parameterization allowed us to estimate sex-adjusted longitudinal changes and the sex difference in longitudinal changes at the same time.

Results

Estimated median changes in cortical thickness for the 40 ROIs are shown for the left and right hemispheres in Fig. 4, which summarizes the main results in a single "dot plot." Here, the black dots give the estimated rates of change and the black lines denote 95% confidence intervals (CIs). If the 95% CI crosses the zero line, then the slopes are not statistically significant. For regions that also show a sex difference, red and blue points are indicated, representing the female and male slopes, respectively. In addition, we also present our results as measures of effect sizes in the various brain regions by deriving the standardized regression coefficient in each cortical region analyzed. The derived estimated slope can therefore be interpreted as the change in standard deviation units in cortical thickness per decade (Supplementary Table 1). Significant longitudinal decreases in cortical thickness were observed in most regions of the left cerebral hemisphere ($p<0.05$). Fewer regions in the right cerebral hemisphere showed statistically significant age-associated longitudinal decreases in median cortical thickness. Two ROIs in the left cerebral hemisphere—the fusiform and lingual gyri—showed significant longitudinal increases in mean cortical thickness. We observe a clear anterior–posterior gradient (Resnick et al., 2003) in the differential rates of decline in cortical thickness across the brain with frontal and parietal regions showing greater rates of decline relative to temporal and occipital regions. This is depicted in Fig. 5 which shows gyral regions on a representative surface colored according to their estimated rates of change.

Analysis of sex differences showed statistically significant differences in rates of cortical thickness changes between males and females in several regions (Fig. 4). These included middle frontal (L), inferior parietal (L), parahippocampal (L), postcentral (L), superior temporal (L), precuneus (R), superior parietal (L and R), and cingulate region (L and R). Males showed consistently greater rates of decline in cortical thickness in these regions in comparison to females.

When we examined nonlinear models of change in the analysis of cortical thickness trends, three ROIs each in the left and right cerebral hemispheres showed significant nonlinear changes over time. These
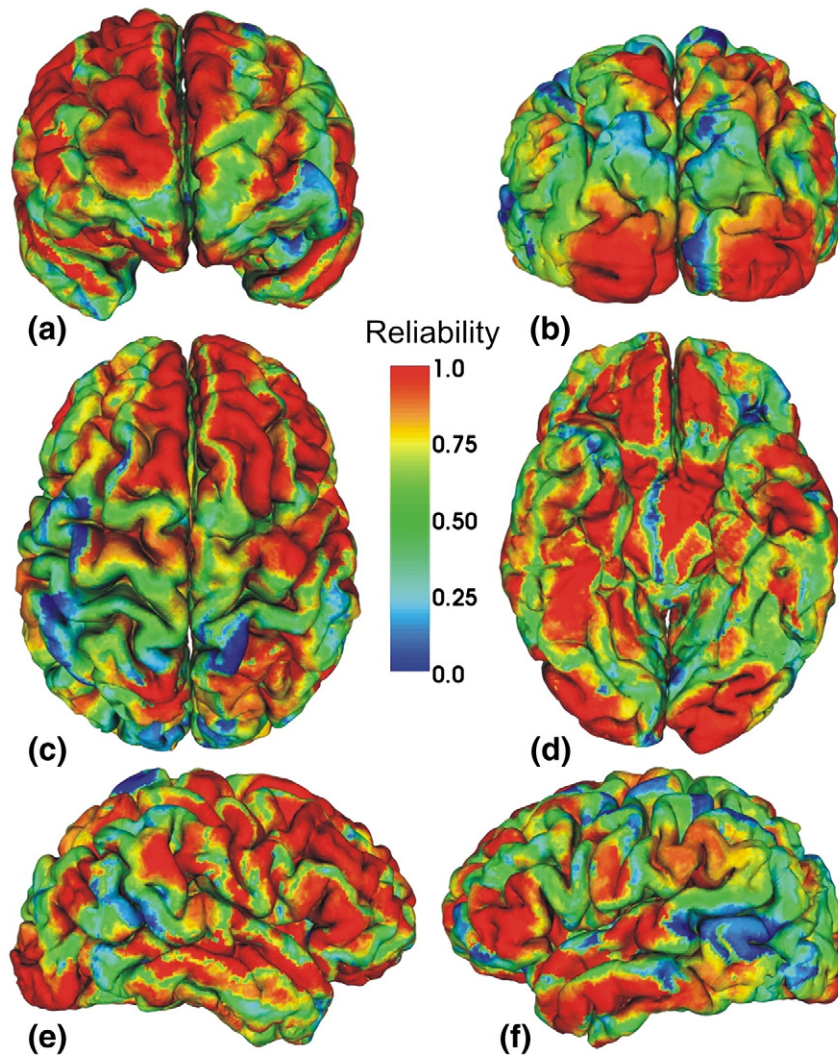
Fig. 3. Reliability map displayed on various views of an outer brain surface.

included the postcentral, precentral, and orbitofrontal gyri on the left and inferior parietal, cingulate, and orbitofrontal gyri in the right cerebral hemisphere, as indicated by the asterisks in Fig. 4.

Discussion

Our principal objective in this study was to delineate the regional distribution of longitudinal changes in thickness across the entire cortical mantle during normal aging in older adults. To accomplish this goal, we analyzed cortical thickness measures in 20 distinct gyral regions of interest (ROIs) in each cerebral hemisphere from 66 non-demented older individuals in the neuroimaging substudy of the BLSA. We derived these data from MRI measures obtained during annual serial neuroimaging with up to 8 annual follow-up assessments. We observe significant and widespread longitudinal declines in cortical thickness during aging, differential rates of decline in distinct cortical regions, and robust differences in rates of cortical thinning in several regions between males and females.

Structural neuroimaging studies of the aging brain have largely focused on volumetric measures of the cerebral cortex (Coffey et al., 1992; Good et al., 2001; Liu et al., 2003; Resnick et al., 2000; Scahill et al., 2003; Tang et al., 2001). This metric is however a composite measure derived from the product of cortical surface area and cortical thickness, each of which may in turn, be differentially affected during aging by a variety of genetic and/or environmental influences

(Panizzon et al., 2009). It is therefore surprising that there have been relatively few studies focusing on the analyses of cortical thickness or surface area as discrete measures in aging. Another feature of the majority of structural neuroimaging studies of the aging brain is their cross-sectional design (Blatter et al., 1995; Courchesne et al., 2000; Pfefferbaum et al., 1994; Sowell et al., 2004). These studies may be somewhat limited in their ability to account for large inter-individual variability to changes in brain structure and are restricted to studying the effect of chronological age on the brain (Fjell et al., 2009). On the other hand, by incorporating data from multiple time points, longitudinal studies are able to address intra-individual effects of the process of aging on brain structure. Such studies have revealed regional patterns of change over time in brain regions that are distinct from those observed in cross-sectional studies alone (Du et al., 2006; Raz et al., 1997).

The main finding in this study is that age-related decline in cortical thickness is widespread, but shows an anterior–posterior gradient with frontal and parietal regions, in general, exhibiting greater rates of decline than temporal and occipital. This observation is in agreement with an earlier study where we showed a similar pattern of longitudinal decline in gray matter volumes across the brain during normal aging (Resnick et al., 2003). Our results are also consistent with an earlier study from our group where we investigated longitudinal changes in a variety of sulcal anatomical measures during normal aging in a subgroup of these older participants over a 4-year
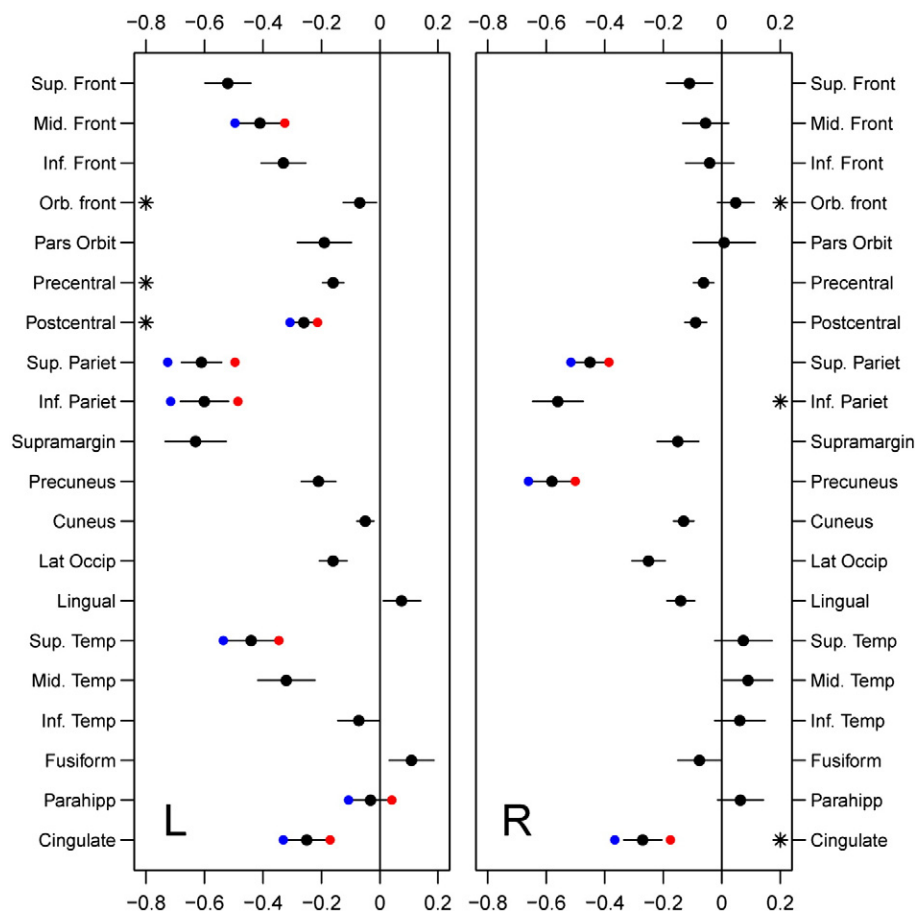
Fig. 4. A dot plot showing median thickness changes by cortical region. The black dots are the estimated sex-adjusted rates of change and the black lines represent the 95% confidence intervals. If the 95% confidence interval crosses the zero line, then the slopes are not statistically significant. For regions that also show a sex difference, red and blue points are also printed, where red and blue are the estimated slopes for females and males, respectively. Units are mm/decade. Asterisks indicate regions showing significant nonlinear changes.

follow-up interval (Rettmann et al., 2006). More recently, a large cross-sectional study on more than 800 individuals ranging in age from 18–93 years demonstrated similar patterns of widespread age-related declines in cortical thickness (Fjell et al., 2009).

It is interesting to note in this context that recent studies suggest that measurements of cortical thickness may be particularly sensitive to early detection of neuropathology within vulnerable brain regions in subjects at risk for AD. A recent cross-sectional study showed that measurements of cortical thickness in the entorhinal cortex (ERC) might be sensitive to detection of pre-symptomatic pathological changes in older individuals at risk for AD (Burggren et al., 2008). Furthermore, this report suggests that measurements of cortical thickness in such individuals may be more sensitive to early pre-clinical pathological changes than standard MRI-based volumetry. Taken together with the findings in our current study, these results may indicate utility of cortical thickness measurements as complementary end points in clinical trials of disease-modifying treatments in subjects at risk for subsequent development of AD.

Our findings of relatively large declines in cortical thickness in the precuneus and cingulate regions are also interesting in the light of previous functional neuroimaging studies that show hypometabolism in these regions to be an early and distinctive feature of AD and mild cognitive impairment (MCI) (Herholz et al., 2007; Matsuda, 2007). This suggests that our observation of decreases in cortical thickness in these regions even in cognitively normal older adults may represent an early and distinct anatomical signature of brain regions at risk for functional decline. In the context of recent neuroimaging studies using the amyloid tracer [11]C[PIB] to study *in vivo* burden of

fibrillar amyloid in the brain, the pattern of decline in cortical thickness observed in the current study appears to be somewhat similar to that of amyloid accumulation in older individuals, affecting predominantly frontal and parietal brain regions more than temporal and occipital (Pike et al., 2007; Rowe et al., 2007). We have recently also combined [^{15}O]water and [11]C [PIB] PET to examine differences in longitudinal changes in regional cerebral blood flow (rCBF) between cognitively normal older individuals dichotomized into those with high and low mean cortical fibrillar amyloid burden. We observed both significant increases and decreases in rCBF in several brain regions between the groups (Sojkova et al., 2008). Interestingly, all the regions exhibiting significant longitudinal changes in rCBF in those with high amyloid burden are those that also show significant declines in cortical thickness in the present study, suggesting at least in some regions that the latter measure is related to changes in brain function during aging.

We also observed significant sex differences in rates of decline in cortical thickness in several brain regions including middle frontal, inferior parietal, superior parietal, postcentral, parahippocampal, precuneus, cingulate, and superior temporal gyri. The pattern of declines in all these regions indicated greater rates of atrophy in men relative to women. This finding is consistent with previous cross-sectional and longitudinal studies, including our own that used volumetric MRI measures to analyze changes in brain volume during normal aging (Coffey et al., 1998; Cowell et al., 1994; Gur et al., 1991; Resnick et al., 2000). Some of these regions, including middle frontal, parahippocampal and superior parietal gyri were also observed to exhibit similar sex differences in rates of atrophy in a recent
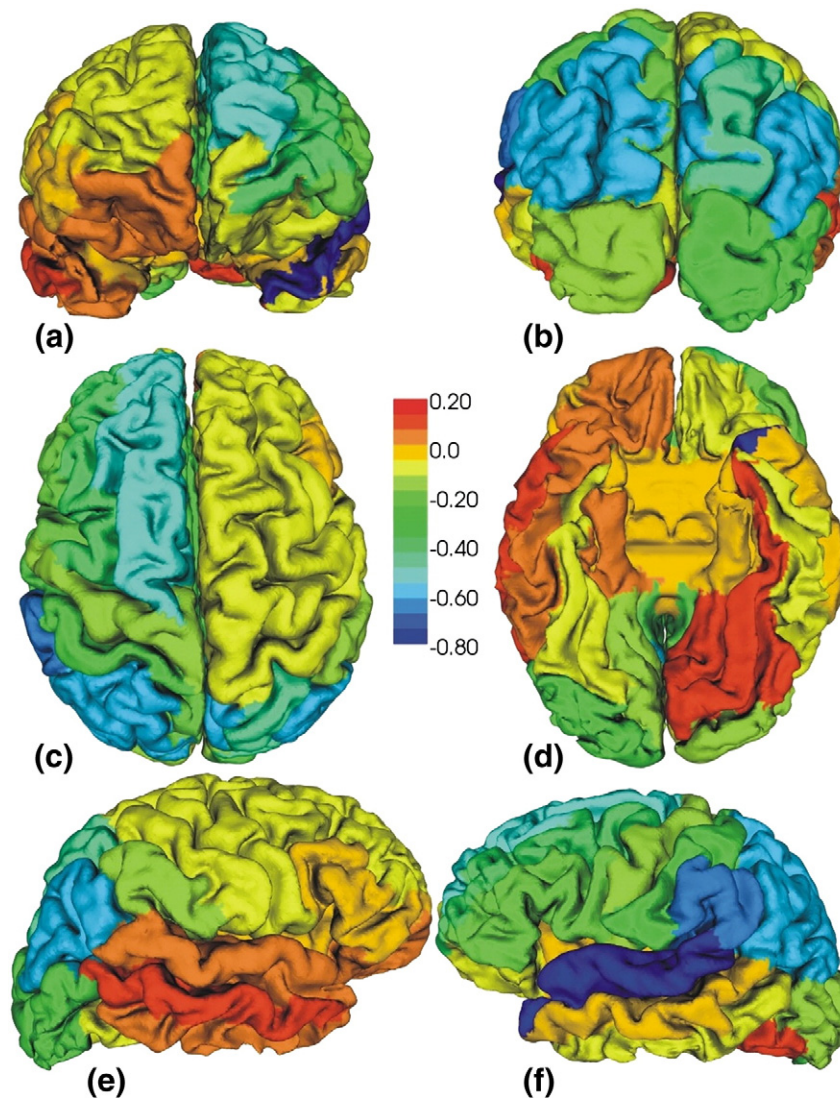
Fig. 5. A typical outer cortical surface with the mean thickness trends for the entire population used to color the entire corresponding gyral region. The color scale is in mm/decade.

longitudinal study of changes in brain volume during normal aging (Driscoll et al., 2009).

Some additional findings in this study that merit consideration include apparent increases in cortical thickness during aging in the left lingual and fusiform regions. Other studies have observed similar increases in the medial frontal region. Although intriguing, we have not directly addressed the likely mechanisms underlying this observation. One plausible explanation may be that decreases in gray white contrast during aging might result in apparent increases in cortical thickness estimates. Our group (Davatzikos and Resnick, 2002) as well as others (Salat et al., 2009) have observed that in some brain regions, statistical effects of changes in gray–white contrast during aging may be stronger than those attributable to cortical thinning (Salat et al., 2009). We also observed striking hemispheric differences in rates of change in cortical thickness in the temporal lobe, with far greater decreases in cortical thickness in the left hemisphere relative to right. Hemispheric asymmetry in patterns of volume changes in the normal aging brain have been previously reported, although these observations have been inconsistent (Raz et al., 2004).

We are aware that some caveats are to be considered in the interpretation of our results. Since our principal aim was to undertake an exploratory analysis of the longitudinal changes in cortical thickness across the entire cortical mantle, we have chosen to present results from all brain regions examined without corrections for multiple hypotheses testing. While this might increase the risk of type-I error, we believe that our approach now allows for further directed analyses of age-related changes in specific brain regions as well as testing *a priori* hypotheses on the role of biological modifiers of such changes. There is also the possibility that substantial effects might occur in a focal region that falls across the boundary of a gyral region and therefore fail to reach significance within either region. Other authors have addressed this problem by performing statistical analysis point-by-point across the entire cortical mantle after registration of multiple subjects to a common atlas (Salat et al., 2004). However, it is important to point out that these methods have the potential to mix registration errors with actual effects, and they also smooth the thickness values by large amounts (e.g., approximating a Gaussian kernel of 22 mm full-width at half-maximum). The net effect of these steps could account for the fact that significance is not achieved in most cortical areas in these other works (see Fig. 3 in Salat et al., 2004). Our approach is fundamentally different in that it pools data from regions that are conceptually registered according to their gyral label, which removes the potential effects of registration errors. Our approach also averages over regions of the cortex in order to reduce noise in thickness measurements, and these regions are histologically meaningful. Our pursuit of this approach was

specifically carried out in order to find more statistically significant relationships than is generally achieved in longitudinal analyses.

It might be asked what effect our particular labeling approach might have on our results. We have run comparisons of our labeling approach against Freesurfer (Makris et al., 2005) and found Dice coefficients falling around 0.75–0.85, which indicates reasonable agreement. Most of the disagreement can be found at the edges of gyral regions in part because Freesurfer gyral boundaries tend to be smoother than ours. The main reason that we investigated the concept of reliability was because of these differences—both variations in our own labeling on different brains as well as the differences between competing methods such as Freesurfer. Though we have not demonstrated this experimentally, we believe that through the use of reliability, our median thickness measurements arise from points on the surface that would in large part be labeled the same by either Freesurfer or CRUISE.

Finally, like other automatic algorithms, CRUISE also shows the gyri around the central sulcus to be thinner than what is expected according to histology. Hutton et al. (2008) speculate that the reason for this difference might be related to contrast differences between gray matter and white matter in this particular region of the brain. We believe that the contrast in this region is not substantially different than elsewhere but that because the histology of these regions is substantially different than others on the cortex—e.g., large Betz neurons and large white matter tracts—the location of the edge of T1 contrast shifts outward. As well, this region provides a very strong edge (though outward from what histology might decide is the actual edge of the gray matter) and it is found very accurately by CRUISE and other automatic algorithms. This may account for the much lower "noise" in the measurements in these regions.

Conclusion

We have undertaken a longitudinal study in cognitively normal older individuals where we derived automated measurements of cortical surface thickness across the entire cortical mantle. Our results show widespread declines in cortical thickness during normal aging and differential rates of cortical thinning in distinct brain regions. In the light of previous functional neuroimaging studies both in normal controls as well as in those with established AD, this study demonstrates the utility of cortical thickness as a potentially useful neuroanatomical correlate of normal and perturbed brain function in health and disease.

Acknowledgments

Appendix A. Supplementary data

Supplementary data associated with this article can be found, in the online version, at doi:10.1016/j.neuroimage.2010.04.258.

References

American Psychiatric Association, 1987. Diagnostic and Statistical Manual of Mental Disorders: DSM-III-R, 3rd ed. American Psychiatric Association, Washington, DC.

Bazin, P.L., Pham, D.L., 2007. Topology-preserving tissue classification of magnetic resonance brain images. IEEE Trans. Med. Imaging 26, 487–496.

Blatter, D.D., Bigler, E.D., Gale, S.D., Johnson, S.C., Anderson, C.V., Burnett, B.M., Parker, N., Kurth, S., Horn, S.D., 1995. Quantitative volumetric analysis of brain MR: normative database spanning 5 decades of life. AJNR Am. J. Neuroradiol. 16, 241–251.

Burggren, A.C., Zeineh, M.M., Ekstrom, A.D., Braskie, M.N., Thompson, P.M., Small, G.W., Bookheimer, S.Y., 2008. Reduced cortical thickness in hippocampal subregions among cognitively normal apolipoprotein E e4 carriers. Neuroimage 41, 1177–1183.

Callen, D.J., Black, S.E., Gao, F., Caldwell, C.B., Szalai, J.P., 2001. Beyond the hippocampus: MRI volumetry confirms widespread limbic atrophy in AD. Neurology 57, 1669–1674.

Coffey, C.E., Wilkinson, W.E., Parashos, I.A., Soady, S.A., Sullivan, R.J., Patterson, L.J., Figiel, G.S., Webb, M.C., Spritzer, C.E., Djang, W.T., 1992. Quantitative cerebral anatomy of the aging human brain: a cross-sectional study using magnetic resonance imaging. Neurology 42, 527–536.

Coffey, C.E., Lucke, J.F., Saxton, J.A., Ratcliff, G., Unitas, L.J., Billig, B., Bryan, R.N., 1998. Sex differences in brain aging: a quantitative magnetic resonance imaging study. Arch. Neurol. 55, 169–179.

Courchesne, E., Chisum, H.J., Townsend, J., Cowles, A., Covington, J., Egaas, B., Harwood, M., Hinds, S., Press, G.A., 2000. Normal brain development and aging: quantitative analysis at in vivo MR imaging in healthy volunteers. Radiology 216, 672–682.

Cowell, P.E., Turetsky, B.I., Gur, R.C., Grossman, R.I., Shtasel, D.L., Gur, R.E., 1994. Sex differences in aging of the human frontal and temporal lobes. J. Neurosci. 14, 4748–4755.

Davatzikos, C., Resnick, S.M., 2002. Degenerative age changes in white matter connectivity visualized in vivo using magnetic resonance imaging. Cereb. Cortex 12 (7), 767–771.

Davatzikos, C., Fan, Y., Wu, X., Shen, D., Resnick, S.M., 2008a. Detection of prodromal Alzheimer's disease via pattern classification of magnetic resonance imaging. Neurobiol. Aging 29, 514–523.

Davatzikos, C., Resnick, S.M., Wu, X., Parmpi, P., Clark, C.M., 2008b. Individual patient diagnosis of AD and FTD via high-dimensional pattern classification of MRI. Neuroimage 41, 1220–1227.

De Santi, S., de Leon, M.J., Rusinek, H., Convit, A., Tarshish, C.Y., Roche, A., Tsui, W.H., Kandil, E., Boppana, M., Daisley, K., Wang, G.J., Schlyer, D., Fowler, J., 2001. Hippocampal formation glucose metabolism and volume losses in MCI and AD. Neurobiol. Aging 22, 529–539.

Desikan, R.S., Segonne, F., Fischl, B., Quinn, B.T., Dickerson, B.C., Blacker, D., Buckner, R.L., Dale, A.M., Maguire, R.P., Hyman, B.T., Albert, M.S., Killiany, R.J., 2006. An automated labeling system for subdividing the human cerebral cortex on MRI scans into gyral based regions of interest. Neuroimage 31, 968–980.

Dickerson, B.C., Bakkour, A., Salat, D.H., Feczko, E., Pacheco, J., Greve, D.N., Grodstein, F., Wright, C.I., Blacker, D., Rosas, H.D., Sperling, R.A., Atri, A., Growdon, J.H., Hyman, B.T., Morris, J.C., Fischl, B., Buckner, R.L., 2008. The cortical signature of Alzheimer's disease: regionally specific cortical thinning relates to symptom severity in very mild to mild AD dementia and is detectable in asymptomatic amyloid-positive individuals. Cereb. Cortex 19 (3), 497–510.

Driscoll, I., Davatzikos, C., An, Y., Wu, X., Shen, D., Kraut, M., Resnick, S.M., 2009. Longitudinal pattern of regional brain volume change differentiates normal aging from MCI. Neurology 72, 1906–1913.

Du, A.T., Schuff, N., Amend, D., Laakso, M.P., Hsu, Y.Y., Jagust, W.J., Yaffe, K., Kramer, J.H., Reed, B., Norman, D., Chui, H.C., Weiner, M.W., 2001. Magnetic resonance imaging of the entorhinal cortex and hippocampus in mild cognitive impairment and Alzheimer's disease. J. Neurol. Neurosurg. Psychiatry 71, 441–447.

Du, A.T., Schuff, N., Zhu, X.P., Jagust, W.J., Miller, B.L., Reed, B.R., Kramer, J.H., Mungas, D., Yaffe, K., Chui, H.C., Weiner, M.W., 2003. Atrophy rates of entorhinal cortex in AD and normal aging. Neurology 60, 481–486.

Du, A.T., Schuff, N., Kramer, J.H., Ganzer, S., Zhu, X.P., Jagust, W.J., Miller, B.L., Reed, B.R., Mungas, D., Yaffe, K., Chui, H.C., Weiner, M.W., 2004. Higher atrophy rate of entorhinal cortex than hippocampus in AD. Neurology 62, 422–427.

Du, A.T., Schuff, N., Chao, L.L., Kornak, J., Jagust, W.J., Kramer, J.H., Reed, B.R., Miller, B.L., Norman, D., Chui, H.C., Weiner, M.W., 2006. Age effects on atrophy rates of entorhinal cortex and hippocampus. Neurobiol. Aging 27, 733–740.

Fjell, A.M., Westlye, L.T., Amlien, I., Espeseth, T., Reinvang, I., Raz, N., Agartz, I., Salat, D.H., Greve, D.N., Fischl, B., Dale, A.M., Walhovd, K.B., 2009. High consistency of regional cortical thinning in aging across multiple samples. Cereb. Cortex 19 (9), 2001–2012.

Fox, N.C., Freeborough, P.A., 1997. Brain atrophy progression measured from registered serial MRI: validation and application to Alzheimer's disease. J. Magn. Reson. Imaging 7, 1069–1075.

Fox, N.C., Warrington, E.K., Freeborough, P.A., Hartikainen, P., Kennedy, A.M., Stevens, J.M., Rossor, M.N., 1996. Presymptomatic hippocampal atrophy in Alzheimer's disease. A longitudinal MRI study. Brain 119 (Pt 6), 2001–2007.

Fox, N.C., Cousens, S., Scahill, R., Harvey, R.J., Rossor, M.N., 2000. Using serial registered brain magnetic resonance imaging to measure disease progression in Alzheimer disease: power calculations and estimates of sample size to detect treatment effects. Arch. Neurol. 57, 339–344.

Good, C.D., Johnsrude, I.S., Ashburner, J., Henson, R.N., Friston, K.J., Frackowiak, R.S., 2001. A voxel-based morphometric study of ageing in 465 normal adult human brains. Neuroimage 14, 21–36.

Gur, R.C., Mozley, P.D., Resnick, S.M., Gottlieb, G.L., Kohn, M., Zimmerman, R., Herman, G., Atlas, S., Grossman, R., Berretta, D., et al., 1991. Gender differences in age effect on brain atrophy measured by magnetic resonance imaging. Proc. Natl. Acad. Sci. U. S. A. 88, 2845–2849.

Han, X., Xu, C., Tosun, D., Prince, J.L., 2001. Cortical surface reconstruction using a topology preserving geometric deformable model. Math. Meth. Biomed. Imag. Anal. Kauai 213–220.

Han, X., Xu, C., Braga-Neto, U., Prince, J.L., 2002. Topology correction in brain cortex segmentation using a multiscale, graph-based algorithm. IEEE Trans. Med. Imaging 21, 109–121.

Han, X., Xu, C., Prince, J.L., 2003. A topology preserving level set method for geometric deformable models. IEEE Trans. Patt. Anal. Mach. Intell. 25, 755–768.

Han, X., Pham, D.L., Tosun, D., Rettmann, M.E., Xu, C., Prince, J.L., 2004. CRUISE: cortical reconstruction using implicit surface evolution. Neuroimage 23, 997–1012.

Hartley, H.O., Rao, J.N.K., 1967. Maximum-likelihood estimation for mixed analysis of variance model. Biometrika 54 (1/2), 93–108.

Herholz, K., Carter, S.F., Jones, M., 2007. Positron emission tomography imaging in dementia. Br J Radiol 80 (Spec No 2), S160–S167.

Hutton, C., De Vita, E., Ashburner, J., Deichmann, R., Turner, R., 2008. Voxel-based cortical thickness measurements in MRI. Neuroimage 40, 1701–1710.

Jack Jr., C.R., Shiung, M.M., Gunter, J.L., O'Brien, P.C., Weigand, S.D., Knopman, D.S., Boeve, B.F., Ivnik, R.J., Smith, G.E., Cha, R.H., Tangalos, E.G., Petersen, R.C., 2004. Comparison of different MRI brain atrophy rate measures with clinical disease progression in AD. Neurology 62, 591–600.

Laird, N.M., Ware, J.H., 1982. Random-effects models for longitudinal data. Biometrics 38, 963–974.

Liu, R.S., Lemieux, L., Bell, G.S., Sisodiya, S.M., Shorvon, S.D., Sander, J.W., Duncan, J.S., 2003. A longitudinal study of brain morphometrics using quantitative magnetic resonance imaging and difference image analysis. Neuroimage 20, 22–33.

Makris, N., Schlerf, J.E., Hodge, S.M., Haselgrove, C., Albaugh, M.D., Seidman, L.J., Rauch, S.L., Harris, G., Biederman, J., Caviness Jr., V.S., Kennedy, D.N., Schmahmann, J.D., 2005. MRI-based surface-assisted parcellation of human cerebellar cortex: an anatomically specified method with estimate of reliability. Neuroimage 25, 1146–1160.

Marcus, D.S., Wang, T.H., Parker, J., Csernansky, J.G., Morris, J.C., Buckner, R.L., 2007. Open Access Series of Imaging Studies (OASIS): cross-sectional MRI data in young, middle aged, nondemented, and demented older adults. J. Cogn. Neurosci. 19, 1498–1507.

Matsuda, H., 2007. The role of neuroimaging in mild cognitive impairment. Neuropathology 27, 570–577.

Misra, C., Fan, Y., Davatzikos, C., 2009. Baseline and longitudinal patterns of brain atrophy in MCI patients, and their use in prediction of short-term conversion to AD: results from ADNI. Neuroimage 44, 1415–1422.

Mungas, D., Harvey, D., Reed, B.R., Jagust, W.J., DeCarli, C., Beckett, L., Mack, W.J., Kramer, J.H., Weiner, M.W., Schuff, N., Chui, H.C., 2005. Longitudinal volumetric MRI change and rate of cognitive decline. Neurology 65, 565–571.

Panizzon, M.S., Fennema-Notestine, C., Eyler, L.T., Jernigan, T.L., Prom-Wormley, E., Neale, M., Jacobson, K., Lyons, M.J., Grant, M.D., Franz, C.E., Xian, H., Tsuang, M., Fischl, B., Seidman, L., Dale, A., Kremen, W.S., 2009. Distinct genetic influences on cortical surface area and cortical thickness. Cereb. Cortex 19 (11), 2728–2735.

Pfefferbaum, A., Mathalon, D.H., Sullivan, E.V., Rawles, J.M., Zipursky, R.B., Lim, K.O., 1994. A quantitative magnetic resonance imaging study of changes in brain morphology from infancy to late adulthood. Arch. Neurol. 51, 874–887.

Pham, D.L., 2001. Robust Fuzzy Segmentation of Magnetic Resonance Images. IEEE Symp on Computer-based Medical Systems, Bethesda, MD, pp. 127–131.

Pike, K.E., Savage, G., Villemagne, V.L., Ng, S., Moss, S.A., Maruff, P., Mathis, C.A., Klunk, W.E., Masters, C.L., Rowe, C.C., 2007. Beta-amyloid imaging and memory in non-demented individuals: evidence for preclinical Alzheimer's disease. Brain 130, 2837–2844.

Pinheiro, J.C., Bates, D.M., 2000. Mixed-Effects Models in S and S-PLUS. Springer, New York.

Raz, N., Gunning, F.M., Head, D., Dupuis, J.H., McQuain, J., Briggs, S.D., Loken, W.J., Thornton, A.E., Acker, J.D., 1997. Selective aging of the human cerebral cortex observed in vivo: differential vulnerability of the prefrontal gray matter. Cereb. Cortex 7, 268–282.

Raz, N., Gunning-Dixon, F., Head, D., Rodrigue, K.M., Williamson, A., Acker, J.D., 2004. Aging, sexual dimorphism, and hemispheric asymmetry of the cerebral cortex: replicability of regional differences in volume. Neurobiol. Aging 25, 377–396.

Resnick, S.M., Goldszal, A.F., Davatzikos, C., Golski, S., Kraut, M.A., Metter, E.J., Bryan, R.N., Zonderman, A.B., 2000. One-year age changes in MRI brain volumes in older adults. Cereb. Cortex 10, 464–472.

Resnick, S.M., Pham, D.L., Kraut, M.A., Zonderman, A.B., Davatzikos, C., 2003. Longitudinal magnetic resonance imaging studies of older adults: a shrinking brain. J. Neurosci. 23, 3295–3301.

Rettmann, M.E., Kraut, M.A., Prince, J.L., Resnick, S.M., 2006. Cross-sectional and longitudinal analyses of anatomical sulcal changes associated with aging. Cereb. Cortex 16, 1584–1594.

Rohde, G.K., Aldroubi, A., Dawant, B.M., 2003. The adaptive bases algorithm for intensity-based nonrigid image registration. IEEE Trans. Med. Imaging 22, 1470–1479.

Rowe, C.C., Ng, S., Ackermann, U., Gong, S.J., Pike, K., Savage, G., Cowie, T.F., Dickinson, K.L., Maruff, P., Darby, D., Smith, C., Woodward, M., Merory, J., Tochon-Danguy, H., O'Keefe, G., Klunk, W.E., Mathis, C.A., Price, J.C., Masters, C.L., Villemagne, V.L., 2007. Imaging beta-amyloid burden in aging and dementia. Neurology 68, 1718–1725.

Salat, D.H., Buckner, R.L., Snyder, A.Z., Greve, D.N., Desikan, R.S., Busa, E., Morris, J.C., Dale, A.M., Fischl, B., 2004. Thinning of the cerebral cortex in aging. Cereb. Cortex 14, 721–730.

Salat, D.H., Lee, S.Y., van der Kouwe, A.J., Greve, D.N., Fischl, B., Rosas, H.D., 2009. Age-associated alterations in cortical gray and white matter signal intensity and gray to white matter contrast. Neuroimage 48, 21–28.

Scahill, R.I., Frost, C., Jenkins, R., Whitwell, J.L., Rossor, M.N., Fox, N.C., 2003. A longitudinal study of brain volume changes in normal aging using serial registered magnetic resonance imaging. Arch. Neurol. 60, 989–994.

Schott, J.M., Price, S.L., Frost, C., Whitwell, J.L., Rossor, M.N., Fox, N.C., 2005. Measuring atrophy in Alzheimer disease: a serial MRI study over 6 and 12 months. Neurology 65, 119–124.

Singh, V., Chertkow, H., Lerch, J.P., Evans, A.C., Dorr, A.E., Kabani, N.J., 2006. Spatial patterns of cortical thinning in mild cognitive impairment and Alzheimer's disease. Brain 129, 2885–2893.

Soininen, H.S., Partanen, K., Pitkanen, A., Vainio, P., Hanninen, T., Hallikainen, M., Koivisto, K., Riekkinen Sr., P.J., 1994. Volumetric MRI analysis of the amygdala and the hippocampus in subjects with age-associated memory impairment: correlation to visual and verbal memory. Neurology 44, 1660–1668.

Sojkova, J., Beason-Held, L., Zhou, Y., An, Y., Kraut, M.A., Ye, W., Ferrucci, L., Mathis, C.A., Klunk, W.E., Wong, D.F., Resnick, S.M., 2008. Longitudinal cerebral blood flow and amyloid deposition: an emerging pattern? J. Nucl. Med. 49, 1465–1471.

Sowell, E.R., Thompson, P.M., Toga, A.W., 2004. Mapping changes in the human cortex throughout the span of life. Neuroscientist 10, 372–392.

Tang, Y., Whitman, G.T., Lopez, I., Baloh, R.W., 2001. Brain volume changes on longitudinal magnetic resonance imaging in normal older people. J. Neuroimaging 11, 393–400.

Tosun, D., Rettmann, M.E., Naiman, D.Q., Resnick, S.M., Kraut, M.A., Prince, J.L., 2006. Cortical reconstruction using implicit surface evolution: accuracy and precision analysis. Neuroimage 29, 838–852.

Wan, J., Carass, A., Resnick, S.M., Prince, J.L., 2008. Automated reliable labeling of the cortical surface. IEEE Int'l Symp Biomed Imaging, Paris, pp. 440–443.

Whitwell, J.L., Josephs, K.A., Murray, M.E., Kantarci, K., Przybelski, S.A., Weigand, S.D., Vemuri, P., Senjem, M.L., Parisi, J.E., Knopman, D.S., Boeve, B.F., Petersen, R.C., Dickson, D.W., Jack Jr., C.R., 2008. MRI correlates of neurofibrillary tangle pathology at autopsy: a voxel-based morphometry study. Neurology 71, 743–749.

Xu, C., Han, X., Prince, J.L., 2000. Improving cortical surface reconstruction accuracy using an anatomically consistent gray matter representation. Functional Human Brain Mapping. NeuroImage, p. S581.